


Attosecond pulse isolation via intense laser field synthesisC. R. J. Fitzpatrick , J. P. Kennedy, B. Dromey, and M. Yeung*Centre for Light-Matter Interaction, Queen's University Belfast, Belfast BT7 1NN, United Kingdom*

(Received 4 April 2023; accepted 14 December 2023; published 23 January 2024)

Precisely synthesized driving fields for relativistic laser-plasma interactions are shown, using particle in cell simulations, to allow for the absolute control over the temporal structure, and efficiency, of emitted attosecond pulse trains. Using a two-color driving field with an off-harmonic frequency as the second color exploits the sensitivity of the generation mechanism to the exact waveform seen by the plasma electrons. Fine control over the relative phase between the two colors, combined with the incommensurate nature of the driving field, breaks the symmetry of the input wave and allows for the selective enhancement of individual pulses in the resultant attosecond pulse train. Our results show that, by suppression of the surrounding pulses in the train, it is possible to use this technique to generate a single isolated attosecond pulse without compromising the resultant intensity as is common in other temporal gating schemes and how it can be combined with the noncollinear gating mechanism to further improve pulse isolation.

DOI: [10.1103/PhysRevResearch.6.L012020](https://doi.org/10.1103/PhysRevResearch.6.L012020)

At the instant a relativistically intense laser field ($I > 10^{18} \text{ W cm}^{-2}$) is incident on a solid density surface, a plasma mirror is formed such that the laser pulse is reflected [1,2]. During this highly nonlinear interaction, electrons at the plasma surface are driven at relativistic velocities and, as a consequence, emit highly coherent extreme ultraviolet (XUV) and x-ray radiation once every cycle of the driving frequency (for oblique incidence) or every half-cycle (for normal incidence). In the case of a multicycle laser, this results in a train of ultrashort pulses on the scale of attoseconds ($1 \text{ as} = 10^{-18} \text{ s}$), represented in the frequency domain as the generation of high-order harmonics [3]. The generation of high-order harmonics and thus a train of attosecond pulses are well described by three distinct mechanisms. Coherent wake emission (CWE), which dominates for moderate intensities with a short plasma scale length [4,5]; coherent synchrotron emission (CSE), which has been shown to efficiently generate bright XUV pulses in normal transmission [6]; and finally the relativistic oscillating mirror model (ROM), which dominates in the highly relativistic regime for comparably longer scale lengths ($L \leq \lambda/10$) [1,7,8].

The potential to harness a single attosecond pulse paves the way for continued development of attosecond science, with applications in real-time ultrafast optical pump-probe experiments to uncover the dynamics of atomic and electronic structures [9,10]. Increasing efforts over the past decade toward attosecond pulse isolation has demonstrated great promise with multiple novel techniques and gating mechanisms. The most obvious approach to obtain a single attosecond pulse is to use a single-to-few cycle incident laser

[11,12], however, achieving single-cycle laser fields becomes extremely challenging with scaling to higher intensities. Other schemes take advantage of temporal gating such as manipulation of the polarization dependence between two noncollinear pulses [13], spatiotemporal gating, which involves streaking the attosecond pulse train in space [14,15], or a combination of different gating mechanisms [16–18].

Previous studies have shown that appropriate tailoring of the waveform of the incident laser field allows control of the shape and periodicity of the up-shifted reflected field. For specific tailoring, it is possible to achieve significant increases in the efficiency of conversion yield to higher harmonics as well as increased pulse intensity [19–22]. While such laser field manipulation has been investigated before, both numerically and experimentally, using the second harmonic of the fundamental frequency, the focus has been on enhancing the intensity of the resultant attosecond bursts of XUV radiation. Here, using 1D and 2D PIC simulations, we present results demonstrating a method of using two-color driving fields to enhance the temporal pulse isolation of the reflected pulse train as seen in the simple schematic in Fig. 1. We show how the use of off-harmonic frequencies as the second color can break the symmetry of the incident field resulting in fine control of the temporal shape of the reflected pulse.

For the results presented in this paper, we simulate two-color incommensurate fields [23,24] incident at 45° on an overdense plasma of $400n_c$, where the critical density $n_c = \omega_p^2 m_e \epsilon_0 / e^2$ with ω_L , m_e , ϵ_0 , and e being the fundamental laser frequency, electron mass, vacuum permittivity, and electron charge, respectively. The incident laser pulse has intensity $a_0 = 20$ where $a_0 = eE_0 / (m_e \omega_L c)$ with E_0 the electric field amplitude and c the speed of light in vacuum. The incident laser pulse has a temporal duration of 17 fs at full width half-maximum (FWHM) and a wavelength of 800 nm. By defining a second pulse with 20% of the total laser intensity, we create a two-color field as the incident laser. Using Lorentz

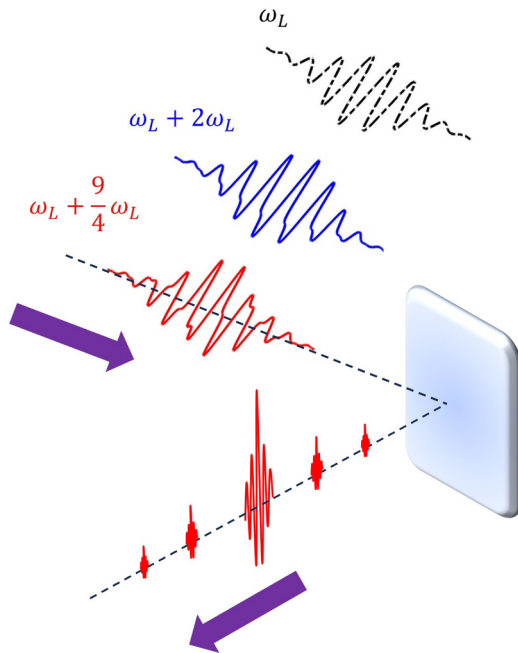


FIG. 1. Simple schematic demonstrating the E_y component of an incommensurate field (red) incident with p polarization on a solid surface. The unique asymmetry (compare with ω_L and $\omega_L + 2\omega_L$ waveforms), with specific relative phases between the two fields results in a temporally isolated attosecond pulse.

transformations, we then boost into a moving frame along the target plane in order to simulate oblique incidence [25] in the 1D PIC code EPOCH [26].

The ability to control the relative phase, $\Delta\phi$, between the two-colour fields allows for precise wave shaping opportunities, and hence, is a key parameter in this setup. A relative phase of zero corresponds to the peaks matching for their central cycle. In order to determine how $\Delta\phi$ dictates the behavior of the reflected pulse train, we performed a parameter scan of $0 < \Delta\phi < 2\pi$ in steps of $\pi/30$. In particular, we compared different off-harmonic frequency multiples of the fundamental as the second color to the case where the second harmonic is used as the extra frequency. The results are shown in Fig. 2.

The top panel in Fig. 2, i.e., (a)–(c), shows a phase scan of $\Delta\phi$ for $2\omega_L$, $(5/2)\omega_L$, and $(9/4)\omega_L$ as the frequency of the second color, respectively. The color map indicates the intensity of the reflected pulses. Harmonics below the 20th have been frequency filtered out from the reflected pulse train (travelling right to left) to remove any low frequency noise, including the fundamental frequency. The red dashed line in each case shows the $\Delta\phi$ value where the central pulse intensity is a maximum which corresponds to the pulse train line outs shown in (g)–(i). It is evident from (a)–(c) the emergence of enhancing and diminishing features in the intensity of the pulse train for particular $\Delta\phi$ values when off-harmonic frequencies are included. For the case where $2\omega_L$ is the second color in (a), the relative amplitudes of each pulse in the train remain constant, regardless of $\Delta\phi$, for example, a clear enhancement for each pulse in the train occurs at $\Delta\phi = 0.266\pi$ while we observe a disruption to each pulse in the train for $\Delta\phi \approx 1.1\pi$ where the maximum pulse intensity is only 5% of the peak case.

Additional simulations were performed to determine the effect of different ratios between the two fields. The results indicated negligible isolation for cases where the second color has a larger fraction of the intensity with optimal isolation when it contains 20% of the energy.

For off-harmonic frequencies we observe that the pulse train behavior is not repeated for each cycle for any given $\Delta\phi$ value. Instead, a disrupted reflected pulse train emerges. In fact, we can predict the distinct behavior of the reflected pulse train by examining the phase of the second color. Equation (1) below describes the condition which, when satisfied, indicates the set of pulses in the train, $N = \{n\} \subseteq \mathbb{N}$, that will experience the same behavior for any one value of $\Delta\phi$,

$$\left(\frac{p}{q}2\pi n\right) \bmod 2\pi = 0. \quad (1)$$

Here, the bracketed term is the phase of the second color with $p, q \in \mathbb{N}$ where their quotient is the off-harmonic frequency. For oblique incidence, we know that an XUV pulse is emitted when $\omega_L t = 2\pi n$, where $\omega_L t$ is the phase of the fundamental frequency and we define $t = 0$ as the time when the central pulse is emitted, with surrounding pulses being emitted every 2π before and after $t = 0$. We can exploit this condition as a method of determining the reflected pulse structure. For the case of an integer multiple used as the second color, $q = 1$, we have $(p2\pi n) \bmod 2\pi = 0$. For any natural number p this holds true $\forall N$, i.e., every pulse will experience the same enhancement or suppression as in Fig. 2(a). Meanwhile, when using an off-integer, $q > 1$, Eq. (1) reads $(2\pi np/q) \bmod 2\pi = 0$. In this case, for the equality to hold for any value of p , we are limited to values of n such that $n/q \in \mathbb{N}$; in other words, n is restricted to multiples of q , that is, $N = \{n \in \mathbb{N} : n = mq\}$ for $m \in \mathbb{N}$. Therefore, not all pulses in the train will experience the same behavior, which is evident in Figs. 2(b) and 2(c), contrary to the integer case. As an example, for $(9/4)\omega_L$ as the second color, $q = 4$, and so in order to satisfy Eq. (1), this means that it's every fourth pulse in the train that undergoes the same characteristic behavior. The relative phase dependence is evidently more intricate, with some pulses in the train being enhanced while the surrounding pulses are suppressed all for one $\Delta\phi$, that is, we observe enhancement coming in and out with respect to the relative phase. It is this complex nature of the off-harmonic phase dependence that provides the control required to isolate ultrashort attosecond pulses. The use of incommensurate fields for this application allows for a time-varying shape of the individual cycles in the incident waveform due to the different periodicity of the off-harmonic frequency used as the second color. This is highlighted in Figs. 2(h)–2(i) which show an increasing temporal gating of the pulse train, resulting in a single intense attosecond pulse. A finer phase scan around the optimal $\Delta\phi$ indicates that, although not perfect, the isolation effect is still present for relative phases either side of the optimal case.

The middle panel in Figs. 2(d)–2(f) represents the time derivative of incident electric field of the laser pulse (travelling left to right) used for each of the three cases presented, where the color map represents the negative gradient of the driving electric field. The gradient of the synthesized laser pulses provides physical insight into the nature of the unique

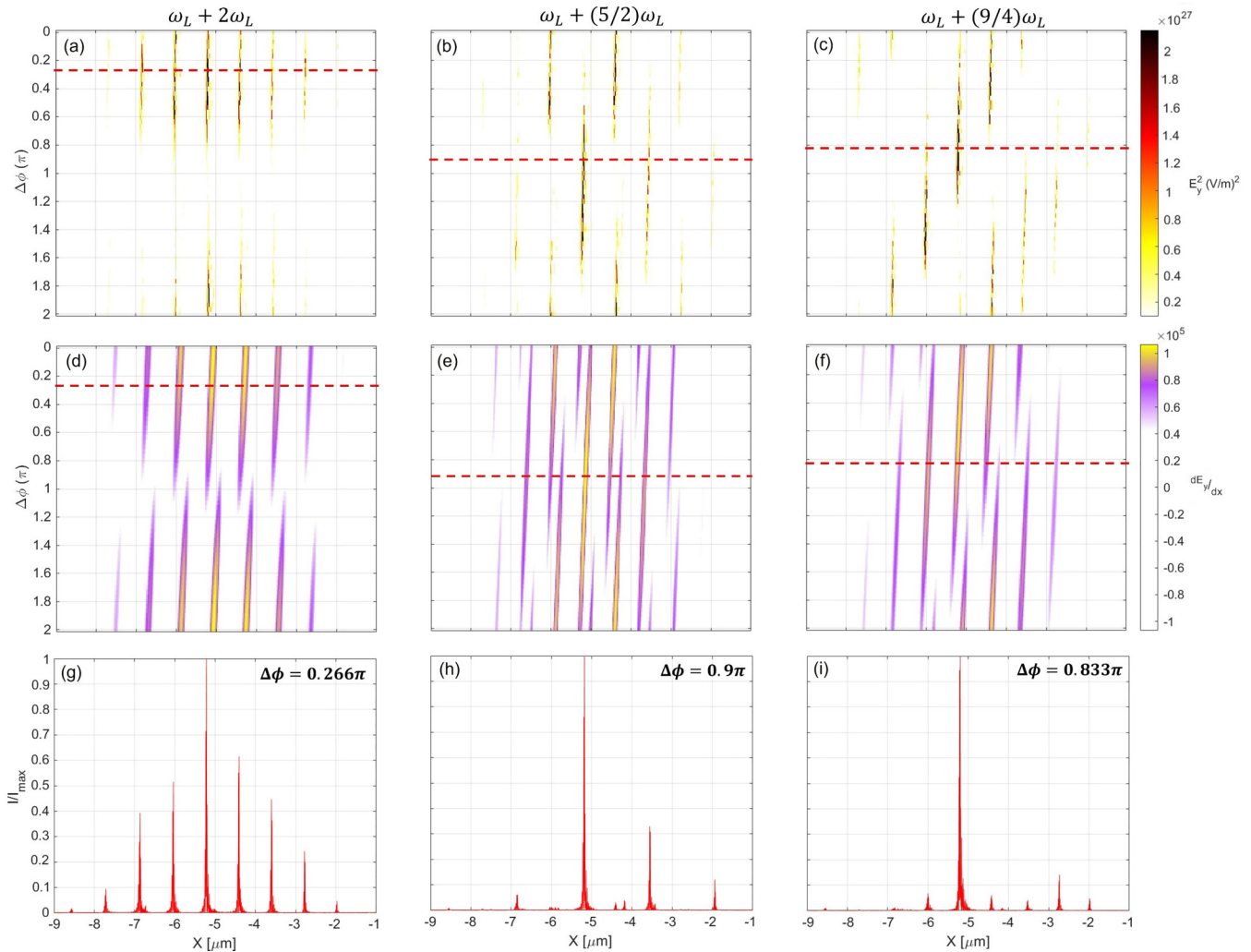


FIG. 2. Simulations demonstrating the resultant pulse structure from off-harmonic wave synthesis. [(a)–(c)] shows a relative phase scan of $0 < \Delta\phi < 2\pi$ for an additional second color of $2\omega_L$, $(5/2)\omega_L$, and $(9/4)\omega_L$, respectively. The color map shows the intensity of the reflected attosecond pulses (right to left). [(d)–(f)] also shows a phase scan but the color map now indicates the negative gradient of the incident laser fields used in [(a)–(c)], respectively. [(g)–(i)] shows the corresponding normalized pulse trains for line outs of the $\Delta\phi$ with the maximum central pulse intensity ($\Delta\phi = 0.266\pi$, 0.9π , and 0.833π for each case). The difference in the pulse structure when using off-harmonic frequencies is demonstrated in (h) and (i) when compared to (g).

reflected pulse trains. The additional bandwidth provided by the off-harmonic frequencies coupled with their asymmetric period with respect to the fundamental allows for a transient phase condition where the driving field experiences an instantaneous switching of direction corresponding to a significant increase in gradient for that one cycle. Comparing the middle panel with the top panel of Fig. 2, we can see that the enhanced pulses in the reflected trains match with when the negative gradient of the laser field is steepest, and indeed the suppression of individual pulses within the train correspond to a comparatively shallow gradient of the incident field.

Figure 3(a) shows the plasma oscillations and XUV pulse emissions with intensity at least 40% of the maximum reflected intensity for $2\omega_L$ with optimum $\Delta\phi$ from Fig. 2(g), that is, where the central pulse has the maximum intensity. As expected, we see that with each oscillation of the plasma surface, an XUV pulse is generated. Simulations show that there are approximately an equal number of electrons in each emitting

bunch, in fact, the highest bunch density is only 1.3 times greater than the average density of the surrounding bunches. Figure 3(b) shows the longitudinal momentum of the emitting bunches labeled 1 and 2 where negative momentum is directed out of the target. It is clear that for adjacent pulses, the bunches undergo a similar trajectory with comparable speeds before returning to the plasma. However, for the $(9/4)\omega_L$ case with the optimized $\Delta\phi$ from Fig. 2(i), only the central pulse is seen to be emitted since the surrounding pulses are less than 40% the maximum, which is also observed in Fig. 3(c) and can be explained by the motion of the electron bunches in Fig. 3(d). Unlike for the $2\omega_L$ case, for adjacent bunches (black), the electrons are moving with approximately four times less momentum than the bunch which is seen to emit an attosecond pulse (red). Here, the highest bunch density is 4.36 times greater than the average of the surrounding bunches. This pairs with previous observations that the emitted XUV power scales with n_b^2 , where n_b is the electron bunch density.

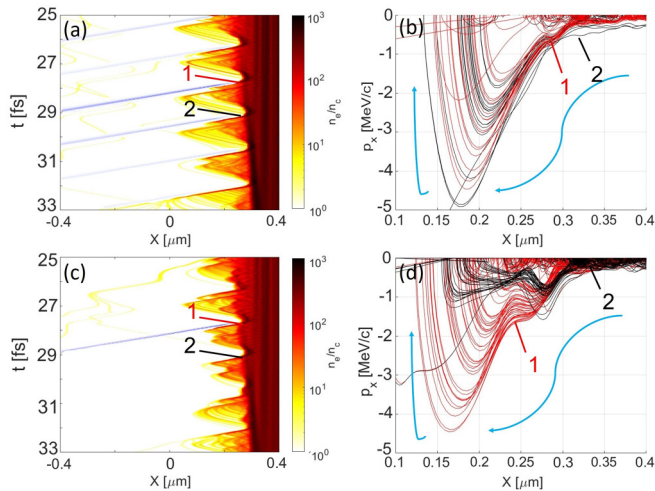


FIG. 3. (a) Plasma surface oscillations with the square of the frequency filtered E-field emissions mapped on top for the dashed line case in Fig. 2(a). Only pulses greater than 40% of the maximum pulse intensity are shown. (b) Longitudinal momentum of the electron bunches for the XUV emission at points 1 and 2. The blue arrows indicate the direction of electron motion under the influence of the tailored laser field. (c), (d) Plasma surface, XUV emission, and longitudinal momentum for the dashed line case in Fig. 2(c). Note the electron momentum and numbers 1 and 2 are color coded to match those points in [(a)–(c)].

Simulations for different off-harmonic colors also indicate the same electron behavior for strong/weak XUV pulses. Note also, that as we continue to add colors of the form $\omega_{SC} = (2n + 1)/n$ for $n \geq 2$, we steadily reduce our bandwidth and approach the case of using the second harmonic $\omega_{SC} = 2\omega_L$.

In order to demonstrate the versatility of this scheme, we performed 2D simulations to investigate the impact of wave synthesis when paired with alternative gating schemes. In particular, we combined it with the recently published non-collinear gating mechanism which uses two pulses, each at an angle θ either side of the target normal and delayed in time, to generate a sweep of attosecond pulses in space [15]. Importantly, our simulations include a longer pulse duration of $\tau = 17$ fs FWHM and a wavelength of $\lambda = 800$ nm in consideration of the currently available laser specifications. We directly compare the results for the best isolation achieved from both the standard noncollinear scheme with that of the combined scheme. In each case, a total laser of $a_0 = 10$ is incident on an overdense plasma of $400n_c$ with scale length $\lambda/20$. Figure 4(a) shows the intensity of the reflected pulse train, filtered for the 20th harmonic and above, sweeping through space for the noncollinear scheme. Below in Fig. 4(c) is the angularly integrated temporal intensity after the electric fields have propagated $150 \mu\text{m}$. Figures 4(b) and 4(d) are analogous to Figs. 4(a) and 4(c) but with the inclusion of $(5/2)\omega_L$ as an additional color to the driving lasers. Figure 4(e) shows the result of filtering, removing the first ten harmonics, after the fields have propagated in both schemes. There is an unambiguous improvement in both the isolation of a single attosecond pulse and the overall intensity, with the combined scheme (red) having an isolated pulse twice as intense and six

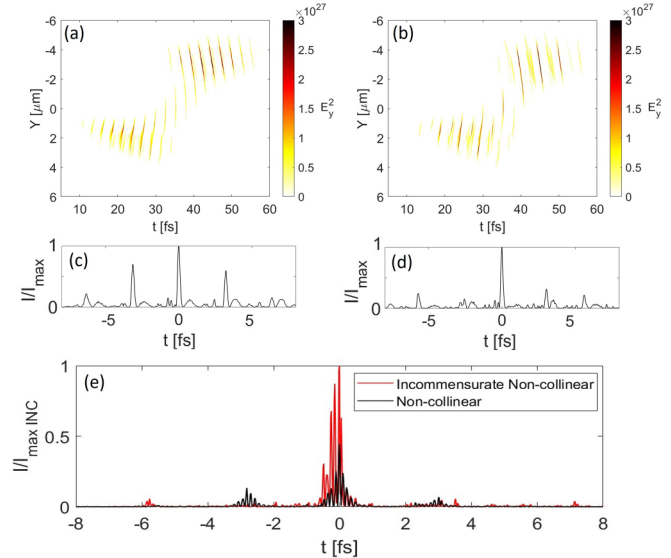


FIG. 4. Visualization of combining the wave synthesis scheme with the noncollinear scheme. (a) and (b) show the filtered reflected intensity and propagated angularly integrated temporal intensity respectively for the noncollinear scheme where the pulses are separated by $7\tau_L$, i.e., seven laser cycles. (c) and (d) show the same results but with the inclusion of an off-harmonic second color of $(5/2)\omega_L$ where the pulses are separated by $6\tau_L$. (e) The reflected train with harmonics 1–10 filtered out for both schemes, showing an excellent isolation of the central pulse with an overall increase in the intensity.

times more isolated than the noncollinear scheme (black). The reason for this increase in intensity is a direct benefit of including the off-harmonic fields. While the noncollinear scheme requires a large temporal delay between the two incident pulses to achieve isolation, this is at the expense of reduced intensity in the overlap region between the two. However, due to the ability of incommensurate fields to suppress the surrounding pulses, we can operate the isolation scheme with a smaller temporal delay between the two lasers while maintaining good isolation, hence an increase in intensity at the point where they overlap. This proves that the effect is not only compatible with different schemes but also beneficial to improve pulse isolation with the bonus of greater pulse intensity.

In conclusion, a method of attosecond pulse isolation from intense laser interactions with plasma surfaces has been demonstrated, which involves the exploitation of off-harmonic frequencies of the fundamental as a second color in the incident laser field. Simulations show that the use of incommensurate fields can change the periodicity of the pulse emission which can be controlled by tuning of the relative phase between the two colors to create a synthesized incident field. Practically, such incommensurate fields have been realized with previous studies using mid-IR lasers to investigate the generation of THz radiation from gas ionization [23,24,27]. In such setups, multiple optical parametric amplifiers (OPAs) are utilised as a source of difference frequency generation [28]. The wavelengths of the output signal and idler beams can then be tuned over large bandwidths based on the angle of incidence between the pump beam and the optical axes of the nonlinear crystal. Additionally, methods

that achieve broadband coherent wave synthesis have been proposed that don't rely on OPA but instead rely on phase and amplitude control modules in particular configurations [29]. The strong attosecond pulse emission is linked to the points of the sharp field gradients in the incident laser, forming electron nanobunches and supporting a strong accelerating field sufficient for XUV radiation. The enhancing and suppressing features observed are explained by the electron trajectories, momentum, and bunch densities in each case. The notable advantage of this scheme is the ability to preserve the intensity of the reflected pulse, allowing for ultrabright ultrashort XUV emission and the ability to be used in tandem with existing gating mechanisms as seen from the 2D simulations. This

gating scheme deepens the understanding of the underlying physics of generating an isolated XUV pulse, helping to further research into probing attosecond science within the relativistic regime.

The data that supports the findings of this study are available upon reasonable request from the authors.

The EPOCH code used in this work was in part funded by the UK EPSRC Grants No. EP/G054940/1, No. EP/G056803/1, No. EP/G055165/1, No. EP/M022463/1, and No. EP/P02212X/1. M.Y. and B.D. acknowledge support from EPSRC Grant No. EP/W017245/1.

-
- [1] G. D. Tsakiris, K. Eidmann, J. Meyer-ter Vehn, and F. Krausz, Route to intense single attosecond pulses, *New J. Phys.* **8**, 19 (2006).
- [2] B. Dromey, M. Zepf, A. Gopal, K. Lancaster, M. Wei, K. Krushelnick, M. Tatarakis, N. Vakakis, S. Moustazis, R. Kodama *et al.*, High harmonic generation in the relativistic limit, *Nat. Phys.* **2**, 456 (2006).
- [3] R. Lichters, J. Meyer-ter Vehn, and A. Pukhov, Short-pulse laser harmonics from oscillating plasma surfaces driven at relativistic intensity, *Phys. Plasmas* **3**, 3425 (1996).
- [4] F. Quéré, C. Thaur, P. Monot, S. Dobosz, P. Martin, J.-P. Geindre, and P. Audebert, Coherent wake emission of high-order harmonics from overdense plasmas, *Phys. Rev. Lett.* **96**, 125004 (2006).
- [5] B. Dromey, S. G. Rykovanov, D. Adams, R. Hörlein, Y. Nomura, D. C. Carroll, P. S. Foster, S. Kar, K. Markey, P. McKenna, D. Neely, M. Geissler, G. D. Tsakiris, and M. Zepf, Tunable enhancement of high harmonic emission from laser solid interactions, *Phys. Rev. Lett.* **102**, 225002 (2009).
- [6] B. Dromey, S. Rykovanov, M. Yeung, R. Hörlein, D. Jung, D. Gautier, T. Dzelzainis, D. Kiefer, S. Palaniypan, R. Shah *et al.*, Coherent synchrotron emission from electron nanobunches formed in relativistic laser-plasma interactions, *Nat. Phys.* **8**, 804 (2012).
- [7] S. V. Bulanov, N. Naumova, and F. Pegoraro, Interaction of an ultrashort, relativistically strong laser pulse with an overdense plasma, *Phys. Plasmas* **1**, 745 (1994).
- [8] T. Baeva, S. Gordienko, and A. Pukhov, Theory of high-order harmonic generation in relativistic laser interaction with overdense plasma, *Phys. Rev. E* **74**, 046404 (2006).
- [9] F. Krausz and M. Ivanov, Attosecond physics, *Rev. Mod. Phys.* **81**, 163 (2009).
- [10] G. Sansone, L. Poletto, and M. Nisoli, High-energy attosecond light sources, *Nat. Photon.* **5**, 655 (2011).
- [11] P. Heissler, R. Hörlein, J. M. Mikhailova, L. Waldecker, P. Tzallas, A. Buck, K. Schmid, C. M. S. Sears, F. Krausz, L. Veisz, M. Zepf, and G. D. Tsakiris, Few-cycle driven relativistically oscillating plasma mirrors: A source of intense isolated attosecond pulses, *Phys. Rev. Lett.* **108**, 235003 (2012).
- [12] F. Quéré, C. Thaur, H. George, J. Geindre, E. Lefebvre, G. Bonnaud, S. Hüller, P. Monot, and P. Martin, Basic mechanisms of laser high-order harmonic generation from plasma mirrors, *J. Mod. Opt.* **55**, 2711 (2008).
- [13] S. G. Rykovanov, M. Geissler, J. Meyer-ter Vehn, and G. D. Tsakiris, Intense single attosecond pulses from surface harmonics using the polarization gating technique, *New J. Phys.* **10**, 025025 (2008).
- [14] H. Vincenti and F. Quéré, Attosecond lighthouses: How to use spatiotemporally coupled light fields to generate isolated attosecond pulses, *Phys. Rev. Lett.* **108**, 113904 (2012).
- [15] J. P. Kennedy, B. Dromey, and M. Yeung, Isolated ultra-bright attosecond pulses via non-collinear gating, *New J. Phys.* **24**, 113004 (2022).
- [16] M. Yeung, J. Bierbach, E. Eckner, S. Rykovanov, S. Kuschel, A. Sävert, M. Förster, C. Rödel, G. G. Paulus, S. Cousens, M. Coughlan, B. Dromey, and M. Zepf, Noncollinear polarization gating of attosecond pulse trains in the relativistic regime, *Phys. Rev. Lett.* **115**, 193903 (2015).
- [17] H. Mashiko, S. Gilbertson, C. Li, S. D. Khan, M. M. Shakya, E. Moon, and Z. Chang, Double optical gating of high-order harmonic generation with carrier-envelope phase stabilized lasers, *Phys. Rev. Lett.* **100**, 103906 (2008).
- [18] N. M. Naumova, J. A. Nees, I. V. Sokolov, B. Hou, and G. A. Mourou, Relativistic generation of isolated attosecond pulses in a λ^3 focal volume, *Phys. Rev. Lett.* **92**, 063902 (2004).
- [19] M. R. Edwards, V. T. Platonenko, and J. M. Mikhailova, Enhanced attosecond bursts of relativistic high-order harmonics driven by two-color fields, *Opt. Lett.* **39**, 6823 (2014).
- [20] M. R. Edwards and J. M. Mikhailova, Waveform-controlled relativistic high-order-harmonic generation, *Phys. Rev. Lett.* **117**, 125001 (2016).
- [21] A. Tarasevitch, J. Wiczorek, R. Kohn, U. Bovensiepen, and D. von der Linde, Two-beam high-order harmonics from solids: Coupling mechanisms, *Phys. Rev. E* **82**, 056410 (2010).
- [22] M. Yeung, S. Rykovanov, J. Bierbach, L. Li, E. Eckner, S. Kuschel, A. Woldegeorgis, C. Rödel, A. Sävert, G. Paulus *et al.*, Experimental observation of attosecond control over relativistic electron bunches with two-colour fields, *Nat. Photon.* **11**, 32 (2017).
- [23] M. Negro, C. Vozzi, K. Kovacs, C. Altucci, R. Velotta, F. Frassetto, L. Poletto, P. Villorosi, S. De Silvestri, V. Tosa *et al.*, Gating of high-order harmonics generated by incommensurate two-color mid-IR laser pulses, *Laser Phys. Lett.* **8**, 875 (2011).
- [24] T. Balciunas, A. Verhoef, A. Mitrofanov, G. Fan, E. Serebryannikov, M. Ivanov, A. Zheltikov, and A. Baltuska,

- Optical and THz signatures of sub-cycle tunneling dynamics, *Chem. Phys.* **414**, 92 (2013).
- [25] A. Bourdier, Oblique incidence of a strong electromagnetic wave on a cold inhomogeneous electron plasma. relativistic effects, *Phys. Fluids* **26**, 1804 (1983).
- [26] T. Arber, K. Bennett, C. Brady, A. Lawrence-Douglas, M. Ramsay, N. Sircombe, P. Gillies, R. Evans, H. Schmitz, A. Bell *et al.*, Contemporary particle-in-cell approach to laser-plasma modelling, *Plasma Phys. Control. Fusion* **57**, 113001 (2015).
- [27] N. V. Vvedenskii, A. I. Korytin, V. A. Kostin, A. A. Murzanev, A. A. Silaev, and A. N. Stepanov, Two-color laser-plasma generation of terahertz radiation using a frequency-tunable half harmonic of a femtosecond pulse, *Phys. Rev. Lett.* **112**, 055004 (2014).
- [28] C. Manzoni, S.-W. Huang, G. Cirimi, P. Farinello, J. Moses, F. X. Kärtner, and G. Cerullo, Coherent synthesis of ultra-broadband optical parametric amplifiers, *Opt. Lett.* **37**, 1880 (2012).
- [29] C. Manzoni, O. D. Mücke, G. Cirimi, S. Fang, J. Moses, S.-W. Huang, K.-H. Hong, G. Cerullo, and F. X. Kärtner, Coherent pulse synthesis: Towards sub-cycle optical waveforms, *Laser Photonics Rev.* **9**, 129 (2015).